Research Article Open Access

Davood Ghanbari*, Samaneh BandehAli, and Abdolreza Moghadassi

Embedded three spinel ferrite nanoparticles in PES-based nano filtration membranes with enhanced separation properties

https://doi.org/10.1515/mgmc-2022-0001
received May 01, 2021; accepted November 10, 2021

Abstract: In this study, three types of ferrites nanoparticles including $CoFe_2O_4$, $NiFe_2O_4$, and $ZnFe_2O_4$ were synthesized by microwave-assisted hydrothermal method. The X-ray diffraction analysis (XRD), Fourier transform infrared spectroscopy (FTIR), and field emission scanning electron microscopy (FESEM) were employed to analyze synthesized nanoparticles and fabricated membranes. The morphology of membrane surface was investigated by surface images. The ability of ferrite nanoparticles was evaluated to the separation of sodium salt and heavy metals such as Cr^{2+}, Pb^{2+}, and Cu^{2+} from aqueous solutions. The modified membrane showed the enhancement of membrane surface hydrophilicity, porosity, and mean pore size. The results revealed a significant increase in pure water flux: 152.27, 178, and 172.68 $L{\cdot}m^{-2}{\cdot}h^{-1}$ for PES/0.001 wt% of $CoFe_2O_4$, PES/0.001 wt% $NiFe_2O_4$, and PES/0.001 wt% $ZnFe_2O_4$ NPs, respectively. Moreover, Na_2SO_4 rejection was reached 78% at 0.1 wt% of $CoFe_2O_4$ NPs. The highest Cr (II) rejection obtained 72% for PES/0.001 wt% of $NiFe_2O_4$ NPs while it was 46% for the neat PES membrane. The Pb(II) rejection reached above 75% at 0.1 wt% of $CoFe_2O_4$ NPs. The Cu(II) rejection was obtained 75% at 0.1 wt% of $CoFe_2O_4$ NPs. The ferrite NPs revealed the high potential of heavy metal removal in the filtration membranes.

Keywords: ferrite nanoparticles, nanofiltration membrane, separation performance, heavy metal removal

1 Introduction

In recent years synthesis of ferrite nanoparticles and their usage in water treatment were described. Ferrites were obtained from various precursors with magnetic properties and attractive in many applications such as digital recording, microwave devices, sensors, catalysis, ferrofluids, and magnetic refrigeration systems. Spinel ferrites as the class of composite metal oxides with superior magnetic materials are containing ferric ions with general structure $M^{2+}Fe_2^{3+}O_4$ (M = Co^{2+}, Ni^{2+}, Zn^{2+}) because of low cost, high efficiency, resistivity, chemical, thermal strengths, tunable shape, magneto-crystalline anisotropy, electrical insulation, high surface area, surface active sites, and high potential in functionalization. The magnetic properties of ferrite depend on the dispersion of the transition metal ions among the cationic sites in the spinel structure (Ahmadian-Fard-Fini et al., 2018; Goodarzi et al., 2017; Hedayati, 2015; Hedayati et al., 2016a, 2016b; Heidary et al., 2017; Nabiyouni et al., 2012).

SF adsorbents are excellent choice for water treatment through the adsorption or degradation process (Ahmadian-Fard-Fini et al., 2019). The ferrite preparation by precursor method is including the blend of ions at the atomic level which its results after thermolysis is usually nanosized ferrites (Ahmadian-Fard-Fini et al., 2020; Hedayati et al., 2016a, 2016b; Kavousi et al., 2018; Kiani et al., 2019).

There are different methods for the production of SF NPs such as polymerized complex, micro-emulsions, and microwave hydrothermal flash method. These techniques have low rate of yield and need to a long time for the process complete. Moreover, some methods have expensive raw materials, high energy demands. But the chemical synthesis methods from aqueous solutions are simple and suitable for mass production. Also, the control of reaction parameters are easy such as pH, complexing agent, and concentration. Among SF NPs, previous studies have been used magnetic nanoparticles for water treatment. Most studies focused on the conventional

*** Corresponding author: Davood Ghanbari,** Department of Science, Arak University of Technology, Arak, Iran;
e-mail: D-ghanbari@arakut.ac.ir
Samaneh BandehAli: Department of Chemical Engineering, Faculty of Engineering, Arak University, Arak 38156-8-8349, Iran
Abdolreza Moghadassi: Department of Chemical Engineering, Faculty of Engineering, Arak University, Arak 38156-8-8349, Iran

iron oxide-based nanoparticles including magnetite (Fe_3O_4), hematite (α-Fe_2O_3), and maghemite (γ-Fe_2O_3). In recent years, the use of SFs has been widely applied as adsorbent to the capture of heavy metal ions. But there are fewer reports in the use of ferrite NPs especially MFe_2O_4 materials in the membrane filtration such as microfiltration, ultrafiltration, nanofiltration, and reverse osmosis. (BandehAli et al., 2019, 2021).

In this here was reported the synthesis of three different ferrite nanoparticles including $CoFe_3O_4$, $NiFe_2O_4$, and $NiFe_2O_4$ for the fabrication of PES-based NF membranes by microwave hydrothermal method. The synthesized nanoparticles and fabricated membranes were analyzed by XRD, FTIR, and FESEM. Furthermore, the surface morphology of the blend membranes was characterized by three-dimensional surface images. The ability of ferrite NPs were examined to separation of sodium salt and heavy metals such as Cr^{2+}, Pb^{2+}, and Cu^{2+} from aqueous solutions.

2 Result and discussion

The separation performance of the membranes was evaluated by a dead-end nano-filtration system in Figure 1 at pressure of 4.5 bar. Initially, the compaction of membranes was occurred at 5 bar for 30 min by deionized water to obtain a steady pure water flux before filtration test. The pure water flux (PWF) was obtained by:

$$J_{w,1} = \frac{V}{A \times t} \tag{1}$$

where $J_{w,1}$ ($L \cdot m^{-2} \cdot h^{-1}$) is the permeate flux, V, A, and t are the volume of water permeate, effective area of membrane (11.94 cm^2), and time (h), respectively.

The rejection followed by Eq. 2:

$$R(\%) = \left(1 - \frac{C_p}{C_f}\right) \times 100 \tag{2}$$

where C_f is feed solution concentration (Na_2SO_4 (1,100 $mg \cdot L^{-1}$) and heavy metals (300 $mg \cdot L^{-1}$)) and C_p is the concentration of permeate solution.

Figure 2 shows the FTIR spectra of $CoFe_2O_4$, $NiFe_2O_4$, and $ZnFe_2O_4$ nanoparticles in the range of 500-4,000 cm^{-1}. The presence of peaks below 600 cm^{-1} is assigned to tetrahedral and octahedral sites respectively in a spinel structure. Moreover, the binds near 600 cm^{-1} are attributed metal-oxygen intrinsic vibrations in tetrahedral complexes which assigned in the about of 565 cm^{-1} for Zn–O and Ni–O, 594 cm^{-1} for Co–O, and the peaks near the 500 cm^{-1} are related to the presence of Fe–O stretching bonds and it is clear in 410 and 414 cm^{-1} for $ZnFe_2O_4$ and $CoFe_2O_4$ NPs, respectively. The peaks around 3,400-3,500 cm^{-1} correspond to the presence of bending and stretching vibration of H–O–H bond in all FTIR spectra.

XRD pattern of ferrite NPs is shown in Figure 3. The XRD analysis of ferrite nanoparticles presents the formation of crystalline structure of nanoparticles. The crystalline size of NPs was calculated by Scherrer equation about 16, 23, and 14 nm for $CoFe_2O_4$, $NiFe_2O_4$, and $ZnFe_2O_4$ NPs, respectively. Furthermore, the average size of ferrite nanoparticles by FESEM images in Figure 3 were obtained 23, 33, and 25 nm for $CoFe_2O_4$, $NiFe_2O_4$, and $ZnFe_2O_4$ nanoparticles, respectively.

The cross-sectional FESEM images of the fabricated membranes: pure PES and PES/$CoFe_2O_4$, PES/$NiFe_2O_4$, and PES/$ZnFe_2O_4$ are illustrated in Figures 4-6. The FESEM images show the asymmetric structure including a thin

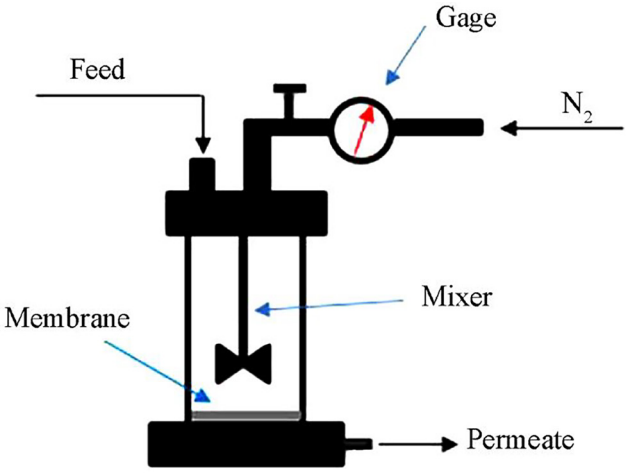

Figure 1: Schematic diagram of the filtration system.

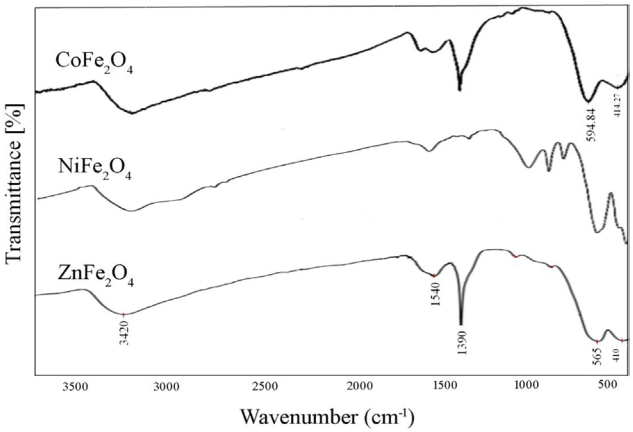

Figure 2: FTIR spectra of ferrite NPs: $CoFe_2O_4$, $NiFe_2O_4$, and $ZnFe_2O_4$.

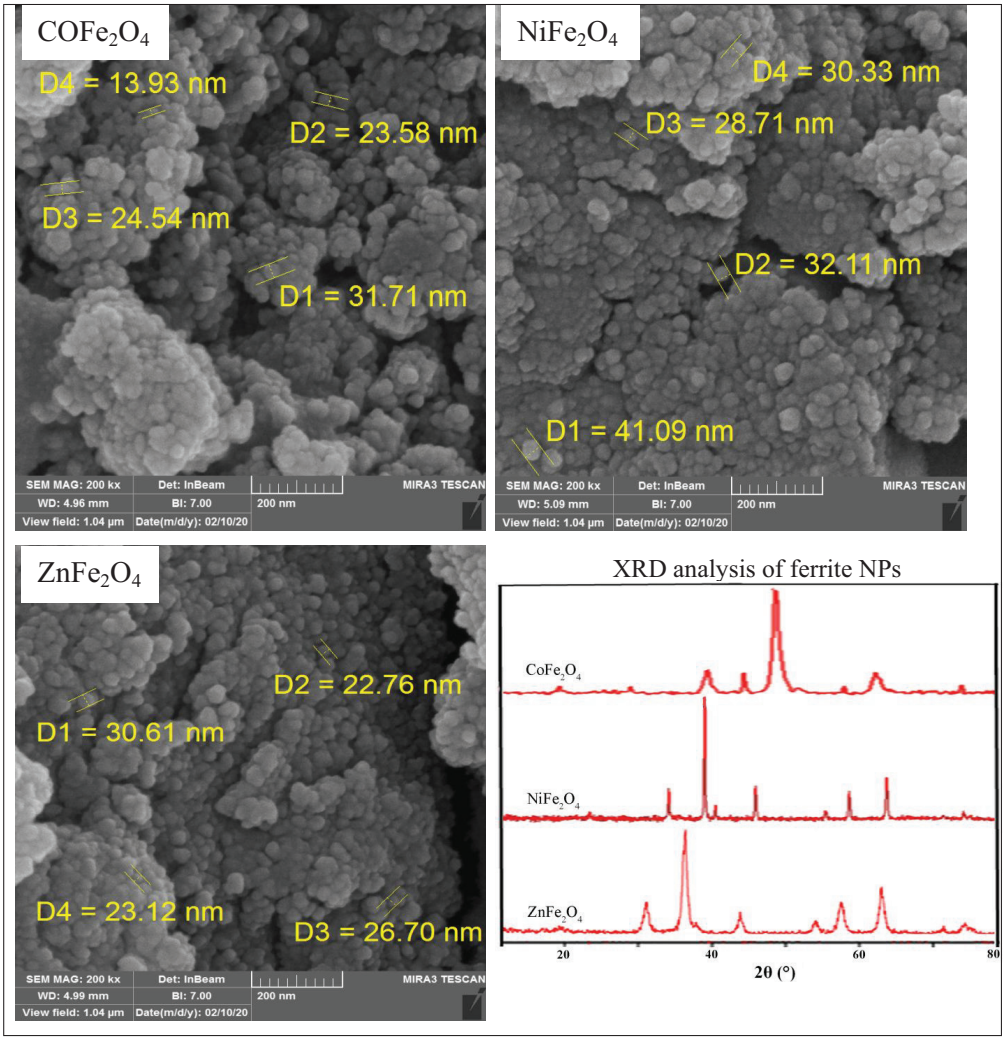

Figure 3: FESEM images and XRD analysis of ferrite NPs: $CoFe_2O_4$, $NiFe_2O_4$, and $ZnFe_2O_4$.

layer on the top of membrane and a finger-like structure as membrane support. This structure forms during an exchange between solvent (dimethylacetamide) and non-solvent (water) in the phase inversion process (Rana et al., 1993, 1996a, 1996b, 2000). Introducing ferrite NPs into the PES membrane change membrane morphology due to thermodynamic and kinetic effects of the system. The presence of nanoparticles disrupts the polymeric chains and reduces the interactions between polymer-polymers. Thus, more voids create into the membrane structure. The introducing nanoparticles into the PES membrane led to the formation of larger and longer pores due to increasing the exchange between solvent and water. As shown in Table 1 and Figure 4, the mean pore size of membrane enhanced to 3.24 nm for 0.01 wt% $CoFe_2O_4$ NPs and then reduced to 1.09 nm at 1 wt% $CoFe_2O_4$ NPs. Moreover, membrane porosity decreased from 70.9% at 0.1 wt% to 65.3% at 1 wt% $CoFe_2O_4$ NPs. These reductions can be attributed to pore filling, increasing solution viscosity. By introducing $NiFe_2O_4$ nanoparticles, did not observe a significant change in the membrane porosity, but increase mean pore size from 1.3 nm for pure PES membrane to 8.67 nm at 0.1 wt% $NiFe_2O_4$ nanoparticles (Table 1 and Figure 5). The decline of mean pore size at 0.01 wt% $NiFe_2O_4$ NPs (M2) can be explained to the bad dispersion of nanoparticles and nanoparticles aggregation into the membrane (Cui et al., 1998; Ghanbari et al., 2016; Khodabakhshi et al., 2018). Furthermore, the man pore size increased from 1.3 nm for the pure PES membrane to 4.56 nm at 0.01 wt% $ZnFe_2O_4$ NPs, then it reduced to 1.6 nm at 1 wt% $ZnFe_2O_4$ NPs due to pore filling with nanoparticles (Table 1 and Figure 6). As shown in FESEM images and Table 1, the introducing $NiFe_2O_4$ nanoparticles create the larger pore compared with another ferrite nanoparticles and the highest membrane porosity obtained for PES/$CoFe_2O_4$ membranes.

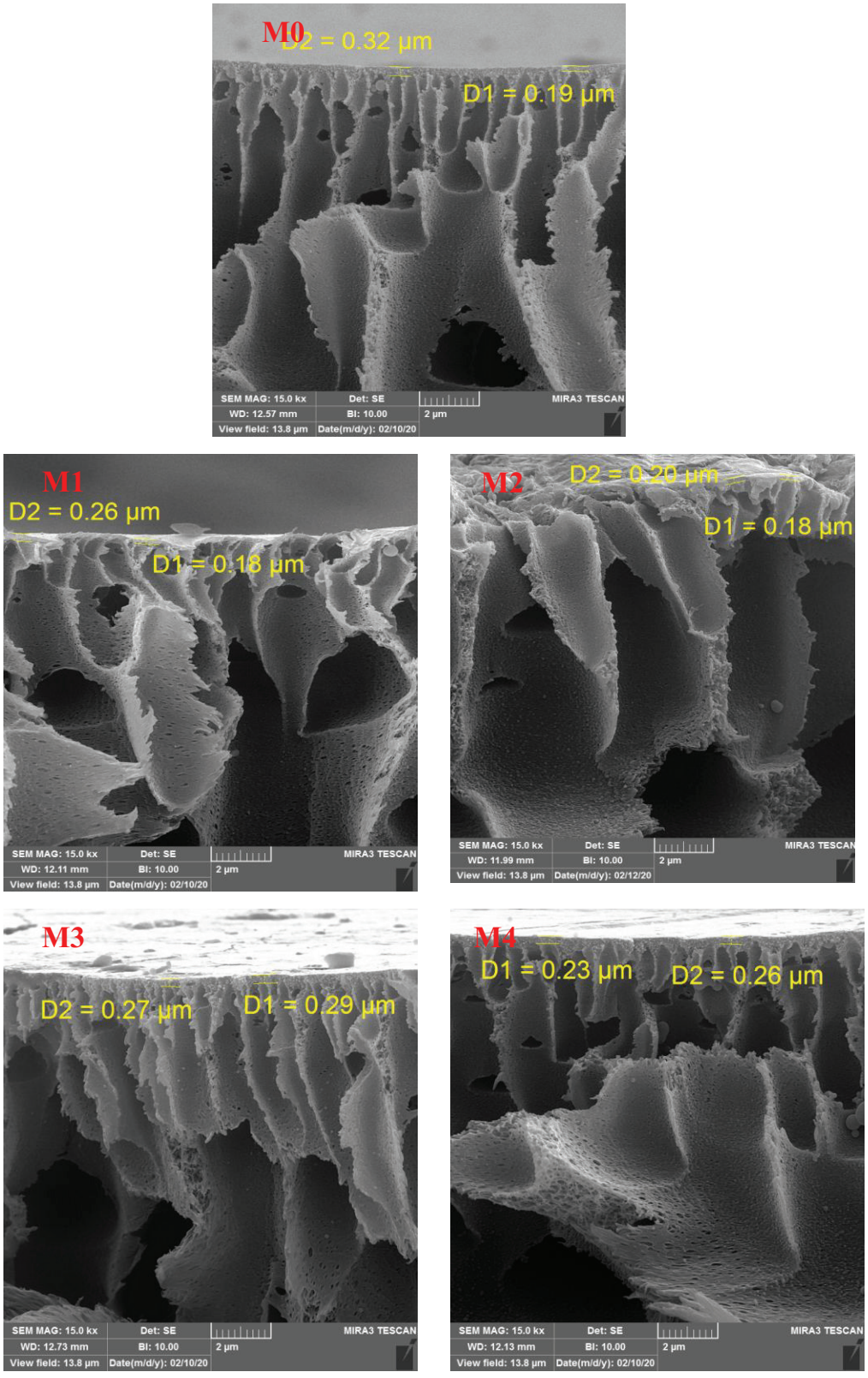

Figure 4: FESEM images of unmodified membrane (M0) and PES/$CoFe_2O_4$ membranes (M1-M4)..

The morphology of the membrane surface and membrane surface roughness was determined by SPM software (version 6.4, Femtoscan). Three-dimensional surface images of the pure PES membrane and modified membranes at 1 wt% of nanoparticle are shown in Figure 7 at scanning area 6 × 6 µm. Moreover, the membrane

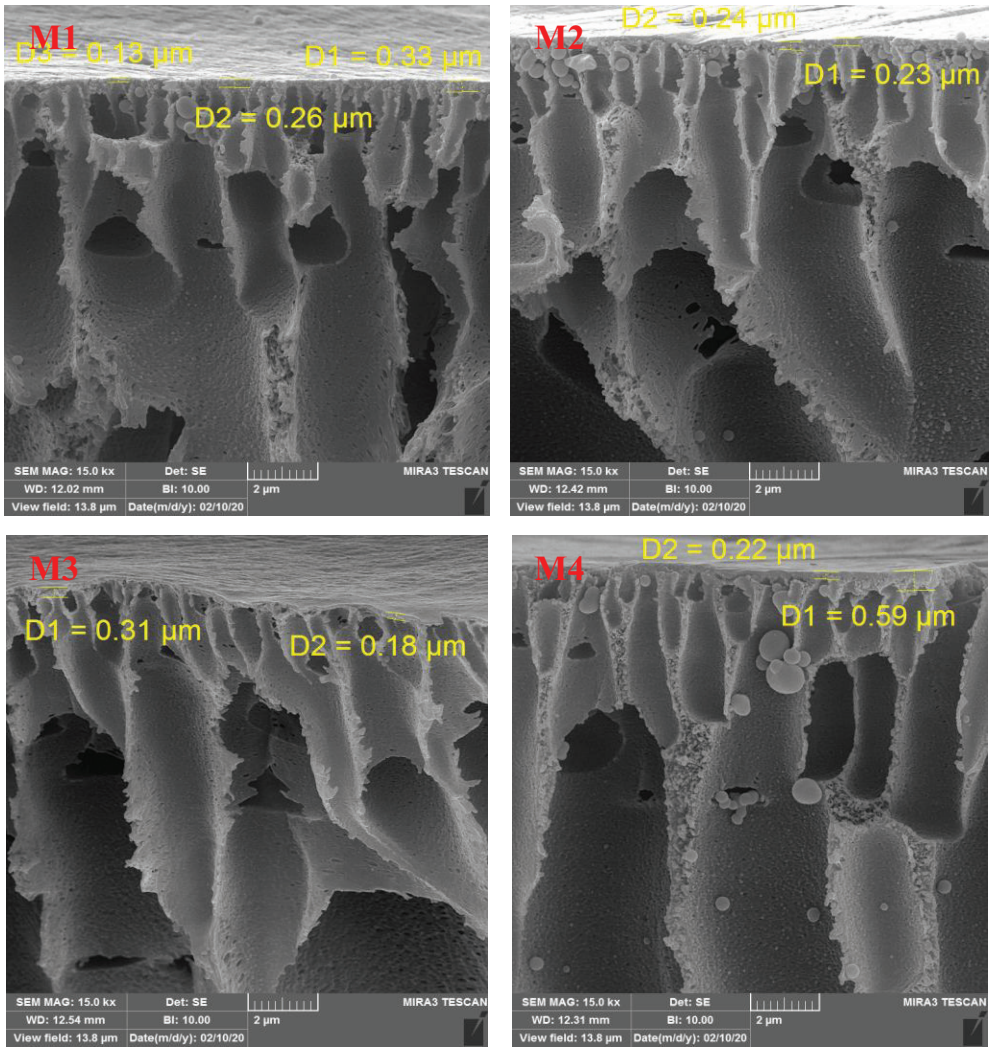

Figure 5: FESEM images of PES/$NiFe_2O_4$ membranes (M1-M4).

roughness parameter including the average roughness (R_a) is presented in Figure 7. According to the results, the modified membranes showed a smoother surface compared with pure PES membrane. By increasing the nanoparticles reduced surface roughness due to pore filling and valleys by the nanoparticles on the membrane surface and then reduction of pore sizes.

The surface hydrophilicty of the fabricated membranes was determined by contact angle and water content measuring (Table 2). All modified membranes showed lower contact angle compared with the pure PES membrane (65°). It is clear that the use of ferrite NPs enhance membrane hydrophilicity and leads to easy transport of the water molecules. Moreover, the highest water content (79%) obtained to PES/1 wt%-$ZnFe_2O_4$ due to its high porosity (79%) (refer to Table 1). The results of the water content showed the increment of water content and membrane hydrophilicity by using ferrite nanoparticles as additive into the PES as the membrane matrix.

Figure 8 indicates PWF of the prepared membranes. It is clear PWF increased significantly compared to the pure PES membrane and the highest PWF was obtained 152, 178, and 172 $L \cdot m^{-2} \cdot h^{-1}$ for PES/0.001 wt% $CoFe_2O_4$, PES/0.001 wt% $NiFe_2O_4$, and PES/0.01 wt% $ZnFe_2O_4$, respectively. This trend is agreement with the increase of mean pore size of the membrane in Table 1. Bigger pores increase water transport and lead to more PWF (Etminan et al., 2018; Ghanbari et al., 2015; Moradi et al., 2018). The decrease of PWF related to decreasing mean pores size and pore filling at high concentration of NPs. Moreover, the formation of interconnect structure of the fabricated membranes is another reason to decline PWF.

Figure 9a shows the Na_2SO_4 rejection for pure PES and three types of modified membranes. Introducing ferrite NPs enhanced Na_2SO_4 rejection to 78%, 72%, and 62% at 0.1 wt% $CoFe_2O_4$, $NiFe_2O_4$, and $ZnFe_2O_4$ NPs. The increase of Na_2SO_4 removal describes with Donnan exclusion effects.

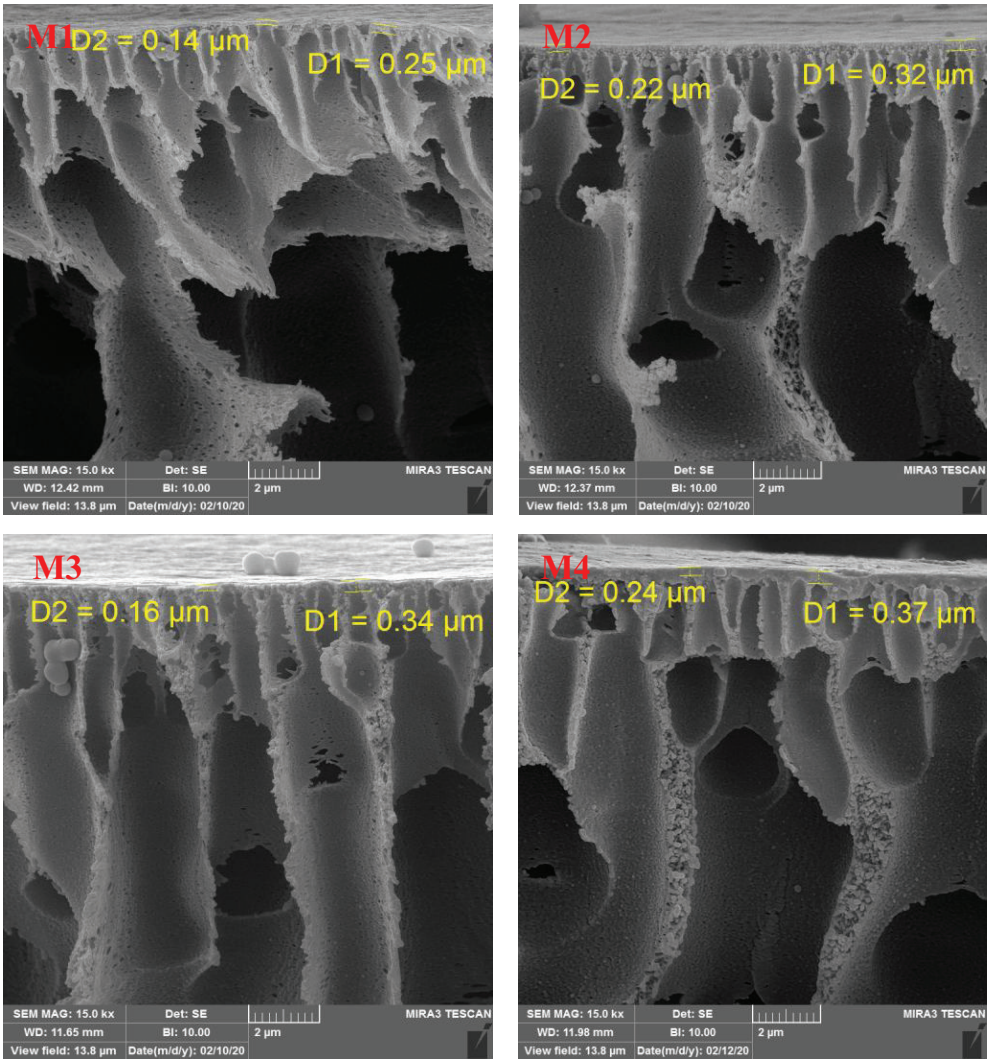

Figure 6: FESEM images of PES/$ZnFe_2O_4$ membranes (M1-M4).

Table 1: Porosity and mean pore size of the pure PES membrane and the modified membranes

Mem.	PES/$CoFe_2O_4$		PES/$NiFe_2O_4$		PES/$ZnFe_2O_4$	
	Porosity (%)	Mean pore size (nm)	Porosity (%)	Mean pore size (nm)	Porosity (%)	Mean pore size (nm)
M0	50	1.3	50	1.3	50	1.3
M1	51.8	5.55	58.9	5.46	50.9	1.29
M2	65.6	3.24	55.5	1.79	35.39	4.56
M3	70.9	1.29	54.5	8.67	48.9	1.75
M4	65.3	1.09	62.3	8.26	79	1.61

Therefore, negative charges on the membrane surface repulse SO_4^{2-} ions. Furthermore, the hydrophilic surface of the modified membranes decreases foulant deposition and concentration polarization which leads to high separation performance. Then Na_2SO_4 rejection reduces in the high concentration of nanoparticles (1 wt%) due to nanoparticle accumulation on the membrane surface. It seems that $CoFe_2O_4$ and $ZnFe_2O_4$ NPs with smaller sizes have better dispersion into the polymeric solution and their membranes have better salt separation than PES/$NiFe_2O_4$ membranes.

Figures 9b,c show the change of Cr(II), Pb(II), and Cu(II) rejection at different concentration of ferrite nanoparticles. The heavy metals removal has an increasing trend. However, the reduction of heavy rejection in high concentration (1 wt%) is due to

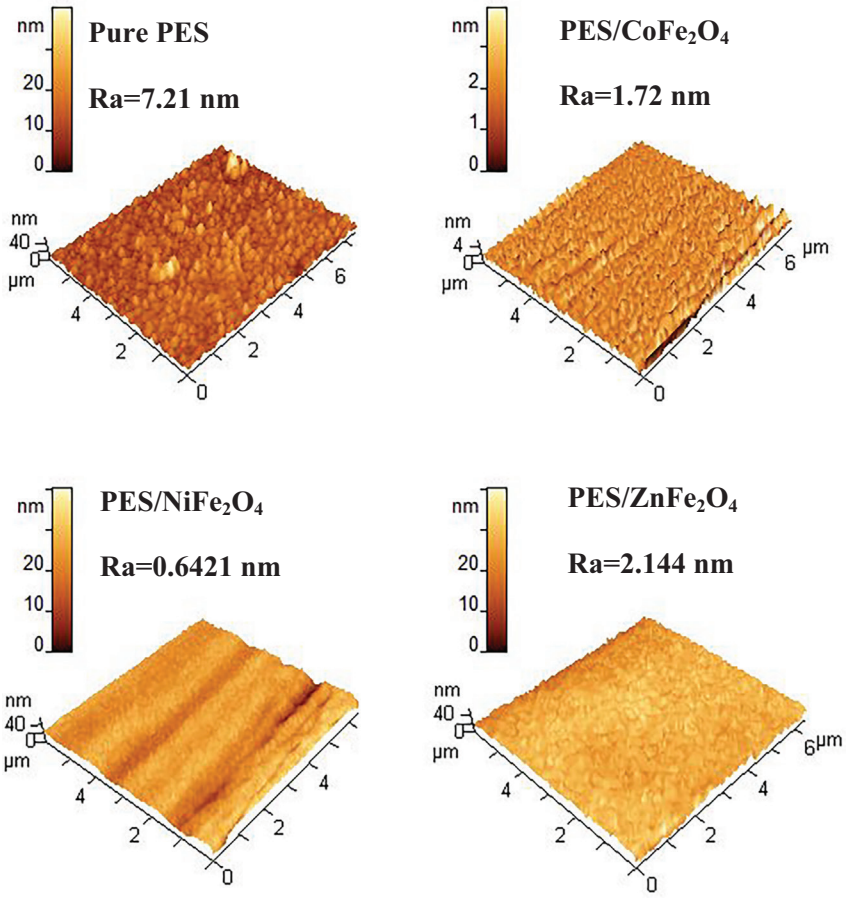

Figure 7: 3D surface images of the pure PES membrane and PES/$CoFe_2O_4$, PES/$NiFe_2O_4$, and PES/$ZnFe_2O_4$ at 1 wt% NPs.

Table 2: Contact angle and water content of all fabricated membranes

Mem.	PES/$CoFe_2O_4$		PES/$NiFe_2O_4$		PES/$ZnFe_2O_4$	
	Contact angle (°)	Water content (%)	Contact angle (°)	Water content (%)	Contact angle (°)	Water content (%)
M0	63	66	63	66	63	66
M1	50	74.6	48	77	51	76
M2	38	78.8	39	72	53	63.7
M3	30	77.2	47	69.9	36	66
M4	39	75.5	28	72.3	44	78.1

accumulation of NPs and decline of active sites to heavy metal adsorption. Cr(II) rejection reached 69% and 68% at 1 wt% Co Fe_2O_4 and $ZnFe_2O_4$ NPs. Moreover, the highest Cr^{2+} rejection was 72% for PES/0.001 wt% $NiFe_2O_4$ while it was 46% for the neat PES membrane. The Pb(II) rejection reach above 75% at 0.1 wt% $CoFe_2O_4$, 0.01 wt% $NiFe_2O_4$, and 0.001 wt% $ZnFe_2O_4$ NPs while it was 45% for the pure PES membrane. Cu(II) rejection obtained 75% and 74% at 0.1 wt% of $CoFe_2O_4$ and $NiFe_2O_4$ NPs. The highest Cu(II) rejection was 74% for PES/1 wt% $ZnFe_2O_4$ membrane while Cu^{2+} rejection was 50% for the pure PES membrane. Mechanisms for the heavy metal rejection are due to the ion electrostatic exclusion via negative charges on the membrane surface and the ion adsorption by NPs. Of course, good dispersion of NPs at suitable values promotes metal ion rejection. It was noticed that ions with a high hydration radius have lower the diffusion coefficient value for the cations in the aqueous solution $Pb^{2+} > Cr^{2+} > Cu^{2+}$. Therefore Pb^{2+} ions transport across the membrane is easier than other metal ions which increase the adsorption capacity of modified membranes due to their spinel structure. Moreover, Cu^{2+} ion removal is higher than Cr^{2+} ions due to the high hydration radius.

3 Conclusion

In this research, $CoFe_2O_4$, $NiFe_2O_4$, and $ZnFe_2O_4$ nanoparticles were synthesized by microwave-assisted hydrothermal method. The various concentrations of synthesized nanoparticles were used to fabricate PES nano-filtration membranes by phase inversion method. FTIR, FESEM, XRD analysis, and three-dimensional surface images were used to analysis membrane and nanoparticles. The separation performance of modified membrane was investigated by sodium salt separation and heavy metals removal. PWF enhanced significantly as well as membrane hydrophilicity and mean pore size of membrane. Modified membrane showed outstanding sodium salt and heavy metal removal and Na_2SO_4, Cr(II), Pb(II), and Cu(II) rejection enhanced 36%, 36%, 40%, and 33% compared with the neat PES membrane.

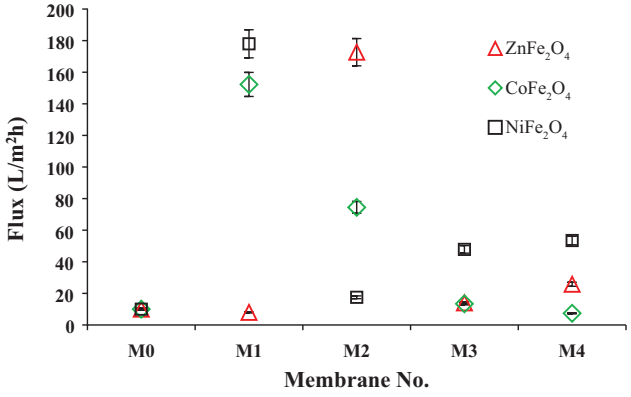

Figure 8: Pure water flux of the pure PES membrane and PES/$CoFe_2O_4$, PES/$NiFe_2O_4$, and PES/$ZnFe_2O_4$ membranes at 4.5 bar pressure.

Experimental

Synthesis of ferrite nanoparticles

Polyethersulfone (PES, M_w = 58,000 g·mol^{-1}) was provided by BASF, Germany, polyvinylpyrrolidone (PVP, M_w = 25,000 g·mol^{-1}) as pores creating agent were provided from Merck, Germany. N, N-dimethylacetamide (DMAc, M_w = 87.12 g·mol^{-1}) as solvent was prepared from DAEJUNG, Korea. $Co(NO_3)_2$, $Ni(NO_3)_2$, $Zn(NO_3)_2$, $Fe(NO_3)_3{\cdot}9H_2O$, and NaOH were prepared from Merck, Germany. Moreover, the aqueous solutions of Na_2SO_4 and $CrSO_4$, $Pb(NO_3)_2$ and $Cu(NO_3)_2$ were provided

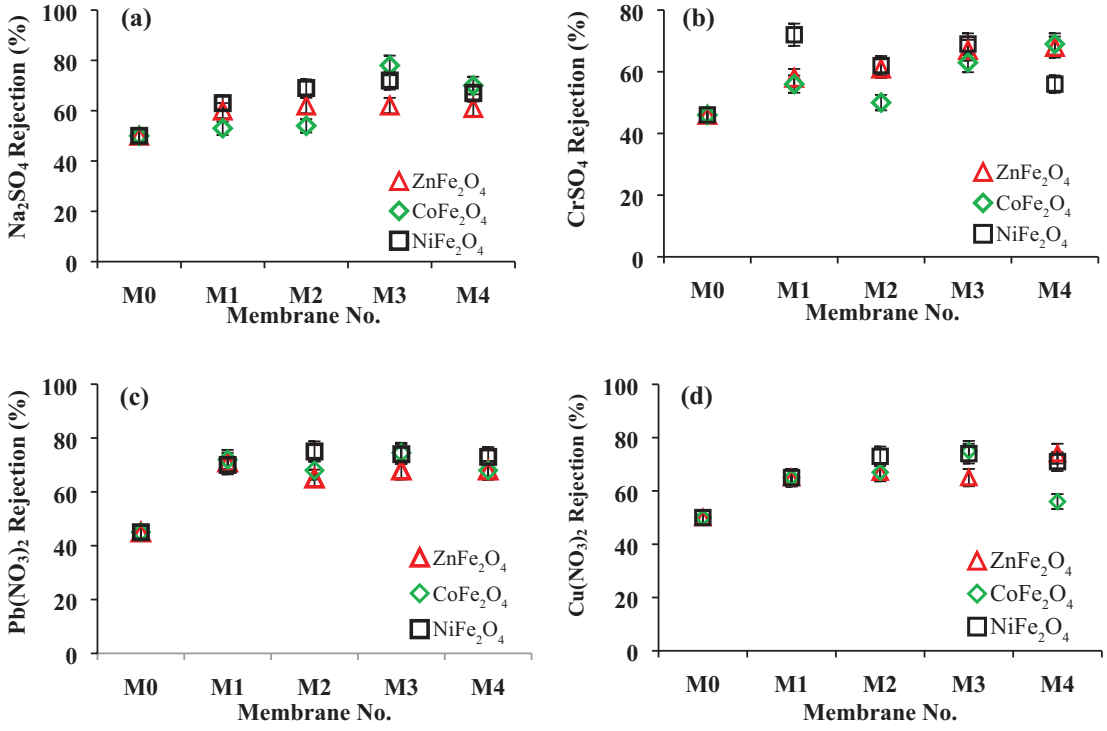

Figure 9: The rejection of Na_2SO_4, $CrSO_4$, $Pb(NO_3)_2$, and $Cu(NO_3)_2$ by the pure PES membrane and PES/$CoFe_2O_4$, PES/$NiFe_2O_4$, and PES/$ZnFe_2O_4$ membranes.

from Merck, Germany for the membrane separation performance analysis.

0.01 mol of $Co(NO_3)_2$, $Ni(NO_3)_2$, and $Zn(NO_3)_2$ were dissolved in the de-ionized water, separately. Then 0.02 mol of $Fe(NO_3)_3{\cdot}9H_2O$ were added to metal solutions in the prior step. Then NaOH solution (1 M) was added to solution (for reaching pH = 10) under microwaves (600 W) for 30 min. After that the solution was heated at autoclave reactor at 180°C for 5 h. The precipitated nanoparticles were centrifuged and washed with distillate water and were placed in oven for drying.

Fabrication of NF membranes

Nanofiltration (NF) membranes were produced through phase inversion method with immersion into the deionized water bath. The polymeric solutions were prepared from PVP (1 wt%) and PES (18%) in DMAc as solvent with different amounts of ferrite nanoparticles. Then casting solutions were stirred for 5 h at room temperature. Polymeric solutions were placed for 40 min in an ultrasonic bath for better dispersion of nanoparticles in solution. The homogeneous solutions conserved for 12 h without stirring in the same temperature due to removing air bubble. Polymeric solutions were cast on a clean glass plates by an applicator and then they were instantly drenched into the distillate water bath. The blend membranes were placed in deionized water for 24 h to remove any soluble material in water and were kept between two filter papers for drying at room temperature. Table 3 indicates the details of the prepared membrane compositions.

Characterization methods

FTIR was applied with a Bruker spectrometer (TENSOR 27) in the range of 400 to 4,000 cm^{-1} at the resolution of 1 cm^{-1} for each spectrum for the characterization of synthesized nanoparticles and membranes. FESEM (SU3500, USA) was employed to determine ferrite NPs and membrane morphology. Moreover, three-dimensional surface image was used to determine the surface morphology of the fabricated membranes in scanning area 6 × 6 μm by SPM software (version 6.4, Femtoscan).

X-ray diffraction pattern (model X' Pert Pw 3373, λ_{Cu} = 0.154°A, Philips, Holland) was used to characterize ferrite nanoparticles. The average size of ferrite crystals (D) was calculated using Debye Scherrer equation in Eq. 3:

$$D_c = \frac{k\lambda}{\beta \cos\theta} \tag{3}$$

where K as a dimensionless value is equal to 0.9, λ is the X-ray wavelength, and β is the full width at half maximum intensity of peak corresponding to 2θ.

The mean pore size and porosity of the membranes was determined by dry-wet weight method. Membranes immersed into the deionized water for 2 h and then weighted. After drying wet membranes, dry weight of membranes was measured. The membranes porosity (ε) and mean pore size of membrane (r_m) were obtained by equations (BandehAli et al., 2019, 2021).

$$\varepsilon(\%) = \left(\frac{W_w - W_d}{\rho_f V_m}\right) \times 100 \tag{4}$$

$$r_m = \sqrt{\frac{(2.9 - 1.75\varepsilon)8\eta LQ}{\varepsilon A \Delta p}} \tag{5}$$

where W_w and W_d are the weight of the wet and dry membrane (g), V_m and ρ_f are membrane volume (cm^3) and water density ($g{\cdot}cm^{-3}$), respectively. η is the water viscosity ($8.9{\times}10^{-4}$ Pa·s), Q is the volume of the permeated water flux ($m^3{\cdot}s^{-1}$), ΔP is operating pressure (0.45 MPa), A is the membrane filtration area (m^2), and L is the thickness of membranes (m).

The contact angle analyzer (G10, Kruss, Germany) was used to the measurement of water contact angle (θ) of membranes. Moreover, the water content of membranes were calculated according to base on wet and dry weight of membranes (BandehAli et al., 2019, 2021):

$$Water\ content\,(\%) = \frac{W_w - W_d}{W_w} \times 100 \tag{6}$$

All experiments were repeated three times and their average values were reported for the decline of the experimental errors.

Table 3: The composition of materials in the membrane preparation

Membrane	PES (wt%)	Ferrite NPs (wt%)	PVP (wt%)	DMAc (wt%)
M0	18	0	1	81.000%
M1	18	0.001%	1	80.999%
M2	18	0.01%	1	80.990%
M3	18	0.1%	1	80.900%
M4	18	1%	1	80.000%

Funding information: Authors state no funding involved.

Author contributions: Davood Ghanbari: writing – review and editing, methodology, experimental analysis; Samaneh BandehAli: writing – original draft, experimental analysis; Abdolreza Moghadassi: writing, resources, project administration.

Conflict of interest: Authors state no conflict of interest.

References

Ahmadian-Fard-Fini S., Ghanbari D., Amiri O., Salavati-Niasari M., Electro-spinning of cellulose acetate nanofibers/Fe/carbon dot as photoluminescence sensor for mercury (II) and lead (II) ions. Carbohyd. Polym., 2020, 229, 115428.

Ahmadian-Fard-Fini S., Ghanbari D., Salavati-Niasari M., Photoluminescence carbon dot as a sensor for detecting of Pseudomonas aeruginosa bacteria: Hydrothermal synthesis of magnetic hollow $NiFe_2O_4$-carbon dots nanocomposite material. Compos. Part B-Eng., 2019, 161, 564-577.

Ahmadian-Fard-Fini S., Salavati-Niasari M., Ghanbari D., Hydrothermal green synthesis of magnetic Fe_3O_4–carbon dots by lemon and grape fruit extracts and as a photoluminescence sensor for detecting of E. coli bacteria. Spectrochim. Acta A., 2018, 203, 481-493.

Bandehali S., Sanaeepur H., Amooghin A.E., Shirazian S., Ramakrishna S., Biodegradable Polymers for Membrane Separation. Sep. Purif. Technol., 2021, 118731.

Bandehali S., Moghadassi A., Parvizian F., Hosseini S.M., A new type of [PEI-glycidyl POSS] nanofiltration membrane with enhanced separation and antifouling performance. Korean J. Chem. Eng., 2019, 36 (10), 1657-1668.

Cui W., Kerres J., Eigenberger G., Development and characterization of ion-exchange polymer blend membranes. Sep. Purif. Technol., 1998, 14, 145-154.

Etminan M., Nabiyouni G., Ghanbari D., Preparation of tin ferrite–tin oxide by hydrothermal, precipitation and auto-combustion: photo-catalyst and magnetic nanocomposites for degradation of toxic azo-dyes. J. Mater. Sci.-Mater. El., 2018, 29, 1766-1776.

Ghanbari D., Salavati-Niasari M., Khaghani S., Beshkar F., Preparation of Polyvinyl Acetate (PVAc) and PVAc–Ag–Fe_3O_4 Composite Nanofibers by Electrospinning Method. J. Clust. Sci., 2016, 27(4), 1317-1333.

Ghanbari D., Salavati-Niasari M., Beshkar F., Amiri O., Electro-spinning of cellulose acetate nanofibers: Microwave synthesize of calcium ferrite nanoparticles and CA–Ag–$CaFe_2O_4$ nanocomposites. J. Mater. Sci.-Mater. El., 2015, 26(11), 8358-8366.

Goodarzi M., Joukar S., Ghanbari D., Hedayati K., $CaFe_2O_4$–ZnO magnetic nanostructures: photo-degradation of toxic azo-dyes under UV irradiation. J. Mater. Sci.-Mater. El., 2017, 28(17), 12823-12838.

Hedayati K., Azarakhsh., Saffari J., Ghanbari D., Photo catalyst $CoFe_2O_4$–CdS nanocomposites for degradation of toxic dyes: investigation of coercivity and magnetization. J. Mater. Sci.-Mater. El., 2016a, 27(8), 8758-8770.

Hedayati K., Azarakhsh S., Ghanbari D., Synthesis and magnetic investigation of cobalt ferrite nanoparticles prepared via a simple chemical precipitation method. J. Nanostruct., 2016b, 6(2), 127-131.

Hedayati K., Synthesis and characterization of nickel zinc ferrite nanoparticles. J. Nanostruct., 2015, 5(1), 13-16.

Heidary F., Khodabakhshi A.R, Ghanbari D., A novel sulfonated poly phenylene oxide-poly vinylchloride/ZnO cation-exchange membrane applicable in refining of saline liquids. J. Clust. Sci., 2017, 28, 1489-1507.

Kavousi F., Goodarzi M., Ghanbari D., Hedayati K., Synthesis and characterization of a magnetic polymer nanocomposite for the release of metoprolol and aspirin. J. Mol. Struct., 2018, 1183, 324-330.

Khodabakhshi A.R., Heidary F., Ghanbari D., Cation Exchange Nanocomposite Membrane Containing $Mg(OH)_2$ Nanoparticles: Characterization and Transport Properties. J. Nanostruct., 2018, 8(2), 191-201.

Kiani A., Nabiyouni G., Masoumi S., Ghanbari D., A novel magnetic $MgFe_2O_4$–$MgTiO_3$ perovskite nanocomposite: Rapid photo-degradation of toxic dyes under visible irradiation. Composite part B: Engineering, 2019, 175, 107080.

Moradi B., Nabiyouni G., Ghanbari D., Rapid photodegradation of toxic dye pollutants: green synthesis of mono-disperse Fe_3O_4–CeO_2 nanocomposites in the presence of lemon extract. J Mater Sci: Mater Electron., 2018; 29 (13), 11065-11080

Nabiyouni G., Boroojerdian P., Hedayati K., Ghanbari D., A simple method for synthesis of PbS nanoparticles using 2-mercapto-ethanol as the capping agent, High. Temp. Mater. Process. 2012, 31 (6), 723-725.

Rana D., Bag K., Bhattacharyya S.N., Mandal B.M., Miscibility of poly(styrene-co-butyl acrylate) with poly(ethyl methacrylate): Existence of both UCST and LCST, J. Polym. Sci., Polym. Phys. Ed., 2000, 38(3), 369-375.

Rana D., Mandal B.M., Bhattacharyya S.N., Analogue calorimetry of polymer blends: poly(styrene-co-acrylonitrile) and poly (phenyl acrylate) or poly(vinyl benzoate). Polymer., 1996a; 37(12): 2439-2443.

Rana D., Mandal B.M., Bhattacharyya S.N., Analogue Calorimetric Studies of Blends of Poly(vinyl ester)s and Polyacrylates, Macromolecules 1996b, 29(5), 1579-1583.

Rana D., Mandal B.M., Bhattacharyya S.N., Miscibility and phase diagrams of poly(phenyl acrylate) and poly(styrene-co-acrylonitrile) blends. Polymer., 1993; 34(7): 1454-1459.